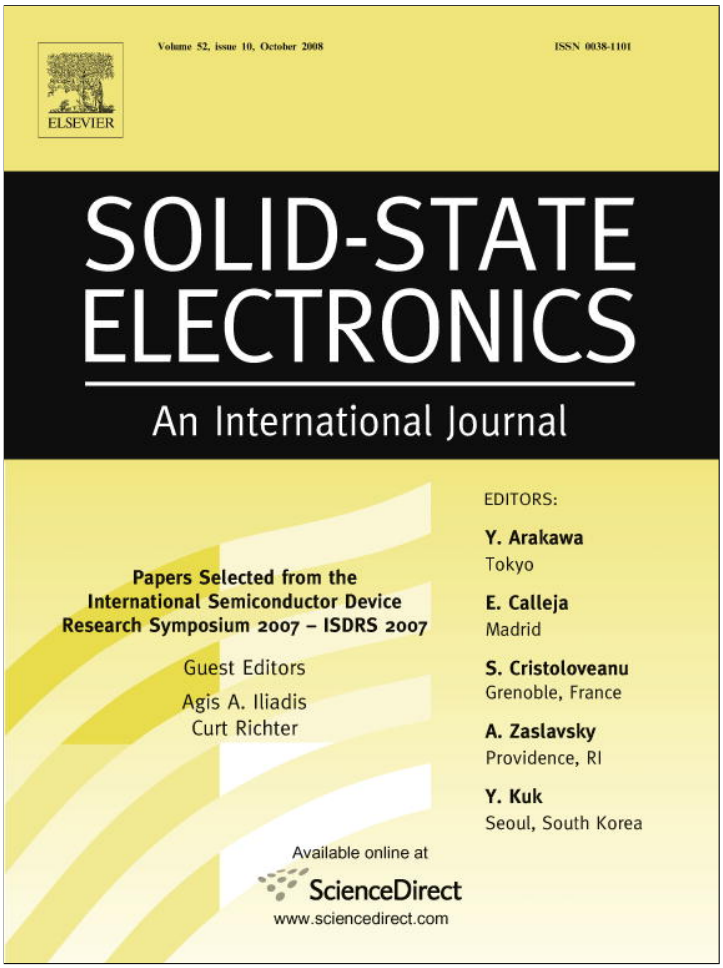

Solid-State Electronics 52 (2008) 1578–1583

Contents lists available at ScienceDirect

Solid-State Electronics

journal homepage: www.elsevier.com/locate/sse

NEMS switch with 30 nm-thick beam and 20 nm-thick air-gap for high density non-volatile memory applications

Weon Wi Jang [a], Jun-Bo Yoon [a,*], Min-Sang Kim [b], Ji-Myoung Lee [b], Sung-Min Kim [b], Eun-Jung Yoon [b], Keun Hwi Cho [b], Sung-Young Lee [b], In-Hyuk Choi [b], Dong-Won Kim [b], Donggun Park [b]

[a] 3D Micro-Nano Structures Lab, Department of Electrical Engineering and Computer Science, Korea Advanced Institute of Science and Technology, Daejeon 305–701, Republic of Korea
[b] Advanced Technology Development Team 1, Semiconductor R&D Center, Samsung Electronics Co., San 24 Nongseo-Dong, Kiheung-Gu, Yongin-City, Kyoungi-Do 449–711, Republic of Korea

ARTICLE INFO

Article history:
Received 18 May 2008
Accepted 7 June 2008
Available online 3 August 2008

Review of this manuscript was arranged by A. Iliadis, C. Richter, and A. Zaslavsky

Keywords:
Nanoelectromechanical systems (NEMS)
Zero off current
Abrupt switching
Suspended beam memory (SBM)

ABSTRACT

We developed two types of titanium nitride (TiN) based nanoelectromechanical systems (NEMS) switches with the smallest dimensions ever made by typical "top-down" complementary metal–oxide–semiconductor (CMOS) fabrication technology. NEMS cantilever switch (NCLS) and NEMS clamp switch (NCS) with 30 nm-thick TiN beam and 20 nm-thick air-gap were successfully fabricated and electrically characterized. The fabricated NCLS showed ideal on/off current characteristics with an essentially zero off current, a sub-threshold slope of less than 3 mV/decade, and an on/off current ratio over 10^5 in air ambient. Also, the NCLS exhibited an endurance of over several hundred of switching cycles under dc and ac bias conditions in air ambient. Suspended beam memory (SBM) cell array structure was suggested for high density non-volatile memory applications.

1. Introduction

Steady scaling of complementary metal–oxide–semiconductor (CMOS) devices has been a significant stimulus for a tremendous advancement in the semiconductor industry over the past four decades. However, many difficult challenges were encountered such as short channel effects, junction leakage and gate oxide leakage as the CMOS design rule is scaled into the nanometer regime [1,2]. Recently, memory devices based on microelectromechanical systems (MEMS) [3–5] and nanoelectromechanical systems (NEMS) [6–9] switches have been reported as one of the promising solutions because they show excellent on/off characteristics due to an essentially zero off current and practically infinite sub-threshold slope, and robustness under harsh environments such as radiation and low/high temperature.

MEMS have already had a noteworthy impact on RF circuit, the automobile, the aerospace and information technology areas [10]. NEMS are a thousand times smaller than MEMS and have the potential to enable revolutionary advances for future applications. Especially, extensive studies have been carried out on NEMS applications of suspended carbon nanotubes (CNTs) due to their superior electrical and mechanical properties [11–18] but existing devices based on the CNTs grown using a "bottom-up" approach are still far from realization due to many obstacles such as difficulty in controlling the position and population of each CNTs.

In this paper, a NEMS cantilever switch (NCLS) and a NEMS clamp switch (NCS) with 30 nm-thick titanium nitride (TiN) beam and 20 nm-thick air-gap were fabricated by a conventional CMOS process. We successfully investigated the electrical characteristics of the two types of NEMS switches showing ideal on/off current property and repetitive operations under dc and ac bias conditions. Moreover, the suspended beam memory (SBM) cell structure based on the NCLS was proposed as one of the promising candidates for high density non-volatile memory applications.

2. Device structure and fabrication

Fig. 1a shows schematics of the two types of NEMS switches. Both the NCLS and the NCS consist of a word line (WL) electrode which is isolated from the adjacent ones by shallow trench isolation (STI) oxide, and a suspended beam hanging over the WL electrode which is anchored on the STI oxide. When applying a voltage between the suspended beam and the WL electrode, the induced electrostatic force pulls the suspended beam down towards the WL electrode, eventually brings it into contact with the WL electrode when the voltage exceeds a certain minimum, so called the pull-in voltage [19]. Consequently, the electric

* Corresponding author. Tel.: +82 42 869 3476; fax: +82 42 869 8565.
E-mail address: jbyoon@ee.kaist.ac.kr (J.-B. Yoon).

0038-1101/$ - see front matter © 2008 Elsevier Ltd. All rights reserved.
doi:10.1016/j.sse.2008.06.026

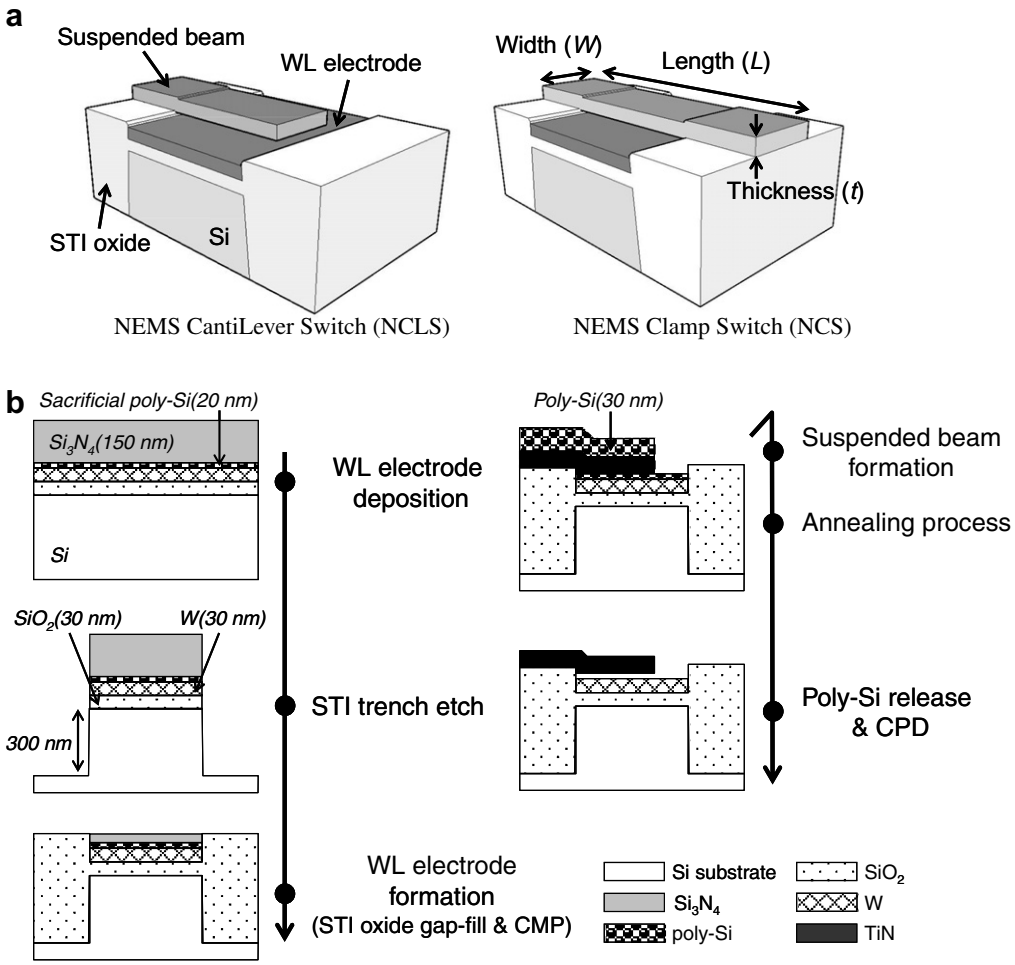

Fig. 1. Schematics of (a) the NCLS and the NCS, which is composed of the WL electrode and the suspended TiN beam and (b) the simplified fabrication process of the NCLS using the conventional "top-down" CMOS process.

current can flow between the suspended beam and the WL electrode.

Fig. 1b illustrates the simplified fabrication process of the NCLS using the conventional CMOS process. All dimensions are indicated in the figure. First, thermally grown silicon dioxide (SiO_2), tungsten (W), sacrificial poly-Si, and silicon nitride (Si_3N_4) hard mask were sequentially deposited on the bulk Si substrate to form the WL electrode. The sacrificial poly-Si was deposited by the thin poly-Si deposition method to obtain an ultra thin and uniform air-gap because the pull-in voltage of the NCLS is dominantly determined by the air-gap thickness. The WL electrode was formed by the conventional shallow trench isolation (STI) method, employing the STI trench etch, STI oxide gap-fill and STI oxide chemical mechanical polishing process. TiN and poly-Si hard mask were deposited to form the suspended beam. We chose a chemical vapor deposited (CVD) TiN as a structure material of the suspended beam because of its unique properties such as a low electrical resistivity of 20 μΩ cm, a high Young's modulus of 600 GPa, and excellent chemical inertness [20]. After an annealing process for relaxing the residual stress of the TiN film, the sacrificial poly-Si was removed by using high selective poly-Si wet etchant and critical point drying process were finally conducted to prevent stiction between the suspended beam and the WL electrode.

Fig. 2a shows top-view scanning electron microscope (SEM) images of the two types of fabricated NEMS switches. The length of the successfully fabricated NCLS and the NCS is about 300 nm and 1000 nm, respectively. As shown in Fig. 2b, the actual thickness of air-gap and suspended TiN beam of the NCLS were measured to be about 20 nm and 30 nm, respectively. The annealing process, which was done before the beam release, successfully eliminated any stress-related deformation of the suspended TiN beam as shown in the inset of Fig. 2b. Consequently, we obtained the ultra thin and uniform air-gap of 20 nm through the wet-release process and the straight suspended TiN beam fabricated using conventional "top-down" process.

3. Results and discussion

Fig. 3a and b shows the *I–V* plots of the two types of fabricated NEMS switches. The NCLS (*W/L/t* = 200 nm/300 nm/30 nm) had a counter-clockwise hysteresis curve with the pull-in voltage of about 13 V and the pull-out voltage of about 8 V, as shown in Fig. 3a. In the case of the NCS (*W/L/t* = 200 nm/1000 nm/30 nm) as shown in Fig. 3b, the pull-in voltage was measured to be about 11 V but an abrupt pull-out characteristics was not clearly shown probably because the force that could restore the long NCS to its original position was not strong enough. In these measurements, a current compliance of 10 nA was used to prevent in-use stiction, which was occurred by Joule heating owing to high current density.

Fig. 4 shows the magnified view of pull-in region of the fabricated NCLS. As soon as the voltage difference between the WL electrode and the suspended beam is over 13.4 V, the electric current begins to rise rapidly to 10 nA. This abrupt switching with less than

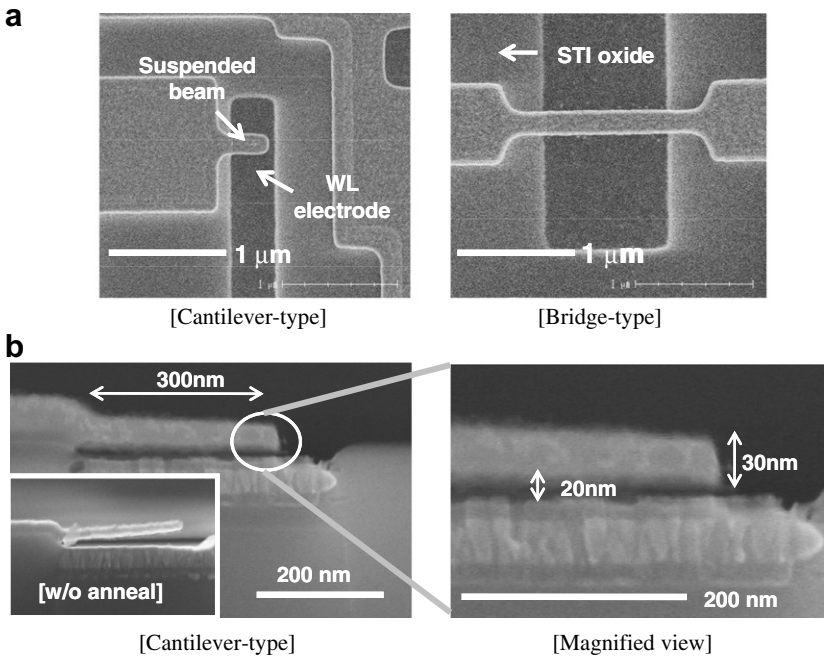

Fig. 2. Scanning electron microscope (SEM) images of (a) top view and (b) cross-sectional view of the fabricated NEMS switches. Inset shows the NCLS without annealing process. The size of the NCLS is 300 nm in length, 200 nm in width and 30 nm in thickness. The size of the NCS with the same thickness is 1000 nm in length and 200 nm in width. The actual air-gap thickness was measured to be 20 nm.

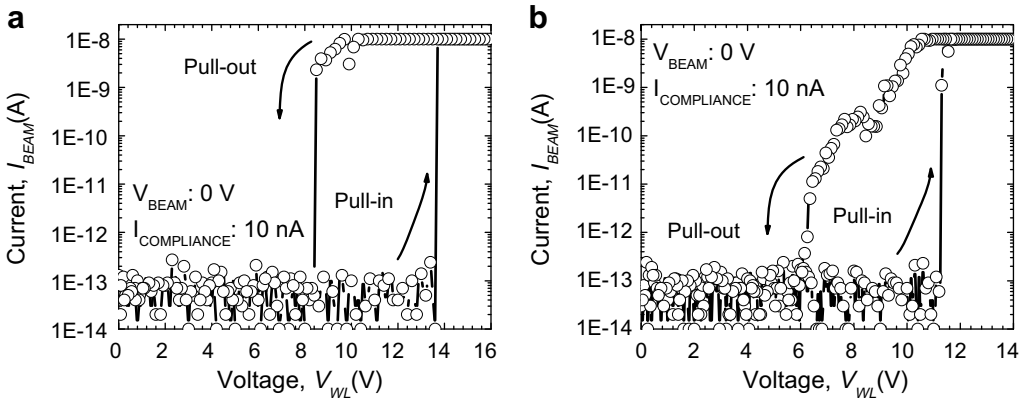

Fig. 3. *I–V* plots of the two types of fabricated NEMS switches for (a) the NCLS ($W/L/t$ = 200 nm/300 nm/30 nm (b) the NCS ($W/L/t$ = 200 nm/1000 nm/30 nm).

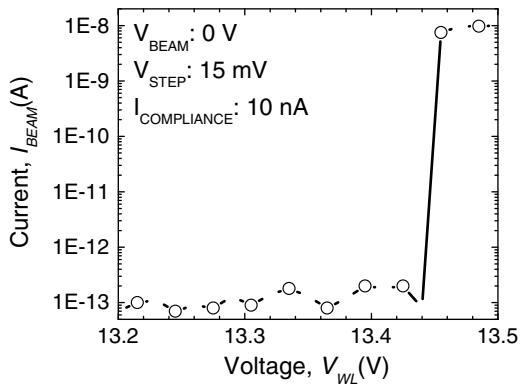

Fig. 4. Magnified view of the pull-in region of the NCLS ($W/L/t$ = 200 nm/300 nm/30 nm), showing ideal on/off current properties.

3 mV/decade (based upon the voltage step of 15 mV and the compliance current of 10 nA, practically infinite) represents ideal on/off current characteristics with an essentially zero off current and an excellent on/off current ratio exceeding 10^5, where the sub-threshold slope is substantially lower than the theoretical limit (60 mV/decade) of CMOS devices at room temperature.

Fig. 5 shows the calculated and measured pull-in voltages of the fabricated NCLS (W/t = 200 nm/30 nm) as a function of suspended beam length. The pull-in voltage of cantilever-type NEMS switch was analytically calculated by using a well-known parallel plate capacitor model [19], which is given by

$$\text{Calculated pull-in voltage } (V_{PI}) = \sqrt{\frac{16t^3g^3E}{81\varepsilon_0 L^4}}$$

where t is the suspended beam thickness, g is the air-gap thickness, E is the Young's modulus, ε_0 is dielectric constant for vacuum, and L

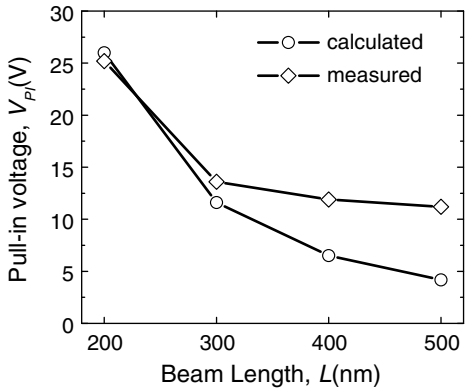

Fig. 5. The calculated and measured pull-in voltages of the fabricated NCLS (W/t = 200 nm/30 nm) as a function of the suspended TiN beam length.

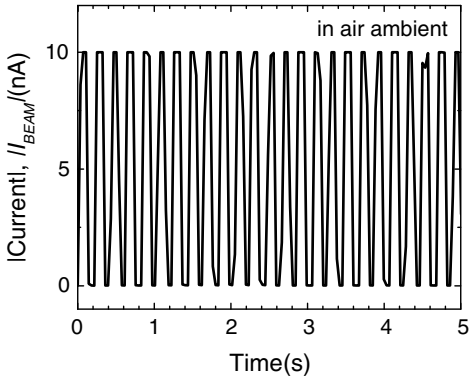

Fig. 7. The beam current of the NCLS as a function of time under ac bias condition in air ambient.

is suspended beam length. Although there is a small error between the measured values and the calculated values by the simple model, the measured pull-in voltages of the NCLS having a length less than 300 nm almost corresponded to the calculated values. However, the measured pull-in voltages become greater than the calculated values of the NCLS having a length longer than 300 nm, where the error is thought to be caused by a slight increase of the air-gap thickness of the long NCLS. We think that even though the annealing process was done, the tensile stress gradient still remained in the CVD TiN film of the NCLS longer than 300 nm causes the suspended beam to bend upward and further optimization of the annealing process will be needed.

Fig. 6a shows the *I-V* plots of the fabricated NCLS under multiple direct current (dc) bias sweep condition in air ambient. The NCLS was repeatedly operated over three hundreds times near the pull-in voltage of 13 V. Also, the measured pull-in voltages are converged into 13 V with the pull-in voltage variation within 1 V as shown in Fig. 6b. Also, we observed that the sub-threshold slope of the NCLS started to deteriorate over certain hundred of switching cycles as the bottom electrode was physically damaged by repeated operations in air ambient.

Fig. 7 shows the electric current of the NCLS as a function of time under alternating current (ac) bias sweep condition in air ambient. Here, an ac bias with a peak voltage of 15 V and a square wave of 5 Hz was applied to the WL electrode and a zero voltage was applied to the suspended beam. The NCLS demonstrates a good pulse response according to an ac signal. Firstly investigated was the endurance of NEMS switch over several hundred of switching cycles under dc and ac bias conditions.

The SBM cell array structure based on the NCLS was proposed for high density non-volatile memory applications as shown in Fig. 8a. The proposed SBM cell consists of a cantilever BL (CBL) connected to a buried BL (BBL) through direct contact (DC), a WL for read (RWL), and a WL for write (WWL) including a charge trapped oxide/nitride/oxide (ONO) layer. The charge can be easily trapped in ONO layer using an ion implantation process during the fabrication or Fowler-Nordheim (FN) tunneling by applying the high voltage between the WWL and the CBL after finishing the fabrication. Fig. 8b and 8c plot the shift of the typical hysteresis curve by the charge trapped in ONO layer, showing the non-volatile memory operation method of the SBM cell. In the case of the SBM cell with the charge trapped ONO layer, the center of the hysteresis curve including the pull-in and pull-out voltage of the SBM cell with the no-charge trapped ONO layer moves on zero voltage owing to the electric field induced by the charge trapped in ONO layer. Therefore, the SBM cell has two bistable states at zero voltage as shown in Fig. 8c: "0" state is that the CBL is initially bent down the ONO layer on the WWL. On the other side, "1" state is that the CBL remains straight. Consequently, "0" and "1" states of the SBM cell are easily distinguished by the position of the CBL.

Fig. 9 shows schematics of the memory operation of the proposed SBM cell. When applying a positive voltage larger than pull-in voltage between the CBL and the WWL, the induced electrostatic force pulls the CBL down towards the ONO layer on the WWL. Eventually, the SBM cell is erased to the "0" state as shown on the left side of Fig. 9a. Therefore, the SBM cell maintains "0" state although the power is off. On the contrary, when a negative

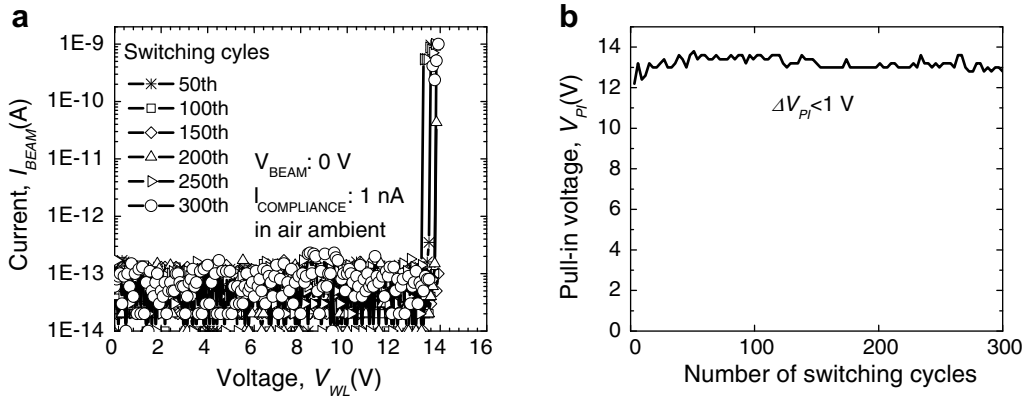

Fig. 6. The *I–V* plots of the fabricated NCLS under multiple dc bias condition in air ambient. The NCLS was repeatedly operated over three hundreds times near the pull-in voltage of 13 V with the pull-in voltage variation within 1 V.

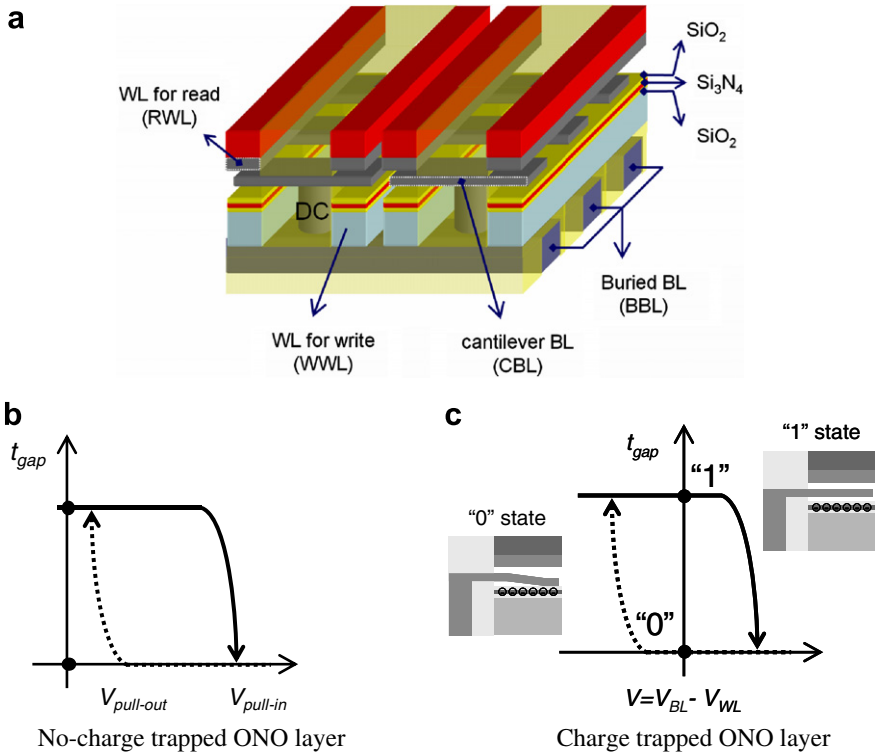

Fig. 8. (a) Schematic diagram of the proposed SBM cell array structure. Hysteresis curves (applied voltage versus air-gap thickness) of the SBM cell with (b) the no-charge trapped ONO layer and (c) the charge trapped ONO layer, showing the operation mechanism of the SBM cell.

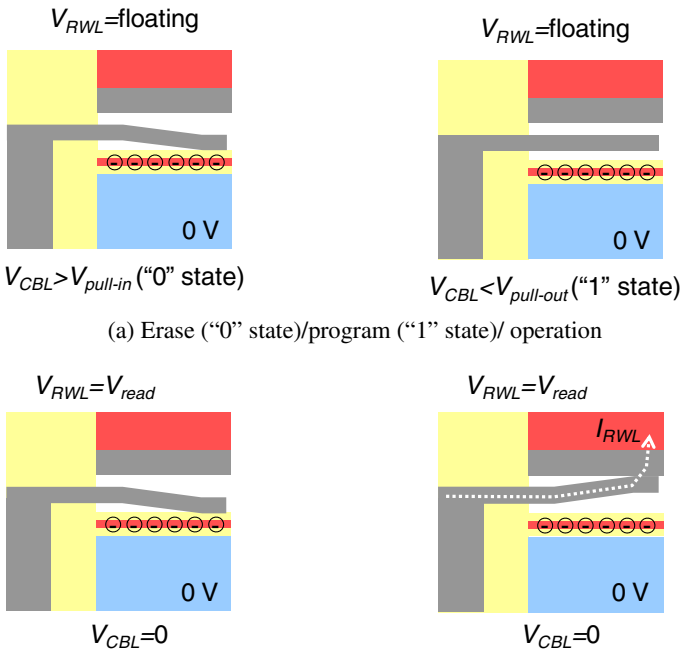

Fig. 9. Schematic diagrams of the (a) erase/program operation and (b) read operation of the proposed SBM cell.

voltage smaller than pull-out voltage is applied between the CBL and the WWL, the CBL is restored to an original position. Then, the SBM cell is programmed to the "1" state as shown on the right side of Fig. 9a. The read operation of the SBM cell is performed by applying the RWL to a positive voltage (i.e., V_{read}) larger than the pull-in voltage between the CBL and the RWL for the programmed SBM cell and smaller than the pull-in voltage between the CBL and the RWL for the erased SBM cell. As shown in the Fig. 9b, the electrostatic force between the CBL and the RWL is large enough to pull upward the CBL to the RWL for the programmed SBM cell,

eventually bringing the CBL into contact with the RWL. Therefore, the electric current flows between the CBL and RWL. In contrast, as the electrostatic force between the CBL stuck to the WWL and RWL is not large enough to pull upward the CBL to the RWL for the erased SBM cell, the no electric current flows between the CBL and RWL because the CBL does not contact to the RWL. Therefore, the memory operation of the SBM cell can be easily realized with complex sensing circuitry. Properly scaling down and using a wafer-level 3D packaging technology, the proposed SBM cell array structure can be expected as one of the promising candidates for high density non-volatile memory applications.

4. Conclusion

The NCLS and the NCS of 30 nm-thick TiN beam and 20 nm-thick air-gap were successfully fabricated using conventional "top-down" CMOS fabrication. The fabricated NCLS demonstrate ideal on/off current characteristics with an essentially zero off current, a sub-threshold slope of less than 3 mV/decade and an excellent on/off current ratio over 10^5 in air ambient. Furthermore, the NCLS showed the repetitive switching operation of over several hundred of switching cycles under ac and dc bias condition in air ambient. We proposed the SBM cell array structure for the high density non-volatile memory applications.

Acknowledgments

This work was supported in 2007 by Samsung Electronics Co., Ltd. and in part the Brain Korea 21 Project of the School of Information Technology at the Korea Advanced Institute of Science and Technology.

References

[1] Meindl JD, Chen Q, Davis JA. Limits on silicon nanoelectronics for terascale integration. Science 2001;293:2044–9.
[2] Frank DJ, Dennard RH, Nowak E, Solomon PM, Taur Y, Wong HSP. Device scaling limits of Si MOSFET's and their application dependencies. Proc IEEE 2001;89:259–88.
[3] Abelé N, Fritschi R, Boucart K, Casset F, Ancey P, Ionescu AM. Suspended-Gate MOSFET: bringing new MEMS functionality into solid-state MOS transistor. IEDM Tech Dig 2005:1075–7.
[4] Kam H, Lee DT, Howe RT, King TJ. A new nano-electro-mechanical field effect transistor (NEMFET) design for low-power electronics. IEDM Tech Dig 2005:477–80.
[5] Jang WW, Lee JO, Yoon JB. A DRAM-like mechanical non-volatile memory. Proc Conf Solid-State Sens & Actuat 2007:153–6.
[6] Rueckes T, Kim K, Joselevich E, Tseng GY, Cheung CL, Lieber CM. Carbon nanotube-based nonvolatile random access memory for molecular computing. Science 2000;289:94–7.
[7] Badzey RL, Zolfagharkhani G, Gaidazhy A, Mohanty P. A controllable nanomechanical memory element. Appl Phys Lett 2004;85:3587–9.
[8] Jang JE, Cha SN, Choi Y, Butler TP, Kang DJ, Hasko DG, et al. Nanoelectromechanical dram for ultra-large-scale-integration (ULSI). IEDM Tech Dig 2005:261–4.
[9] Beunder MA, Kampen RV, Lacey D, Renault M, Smith CG. A new embedded NVM technology for low power, high temperature, rad hard applications. Proc Non-volatile Memory Tech Symp 2005:65–8.
[10] Kovacs GTA. Micromachined transducers sourcebook. New York: HCB/McGraw-Hill; 1998.
[11] Dequesnes M, Rotkin SV, Aluru NR. Calculation of pull-in voltages for carbon nanotube-based nanoelectromechanical switches. Nanotechnology 2002;13:120–31.
[12] Jonsson LM, Axelsson S, Nord T, Viefers S, Kinaret JM. High-frequency properties of a CNT-based nanorelay. Nanotechnology 2004;15:1497–502.
[13] Ke C, Espinosa HD. Feedback controlled nanocantilever device. Appl Phys Lett 2004;85:681–3.
[14] Hollingsworth JP, Bandaru PR. Carbon nanotube based nonvolatile memory. Appl Phys Lett 2005;87:233115.
[15] Kaul AB, Wong EW, Epp L, Hunt BD. Electromechanical carbon nanotube switches for high-frequency applications. Nano Lett 2006;6:942–7.
[16] Hwang HJ, Kang JW. Carbon-nanotube-based nanoelectromechanical switch. Physica E 2005;27:163–75.
[17] Kang JW, Jiang Q. Electrostatically telescoping nanotube nonvolatile memory device. Nanotechnology 2007;18:095705.
[18] Lee SW, Lee DS, Morjan RE, Jhang SH, Sveningsson M, Nerushev OA, et al. A three-terminal carbon nanorelay. Nano Lett 2004;4:2027–30.
[19] Rebeiz GM. RF MEMS theory, design, and technology. Hoboken, NJ: Wiley; 2003.
[20] Seneviratne D, Nielson GN, Takahashi S, Barbastathis G, Tuller HL. On the use of titanium nitride as structural material in nano-electro-mechanical systems (NEMS). Proc IEEE Conf Nanotech 2005:138–41.